

# CityLoc: 6 DoF Localization of Text Descriptions in Large-Scale Scenes with Gaussian Representation

Qi Ma<sup>1,2</sup> Runyi Yang<sup>2</sup> ✉ Bin Ren<sup>2,3,4</sup> Ender Konukoglu<sup>1</sup> Luc Van Gool<sup>1,2</sup> Danda Pani Paudel<sup>2</sup>  
<sup>1</sup>Computer Vision Lab, ETH Zurich <sup>2</sup>INSAIT, Sofia University  
<sup>3</sup>University of Pisa <sup>4</sup>University of Trento

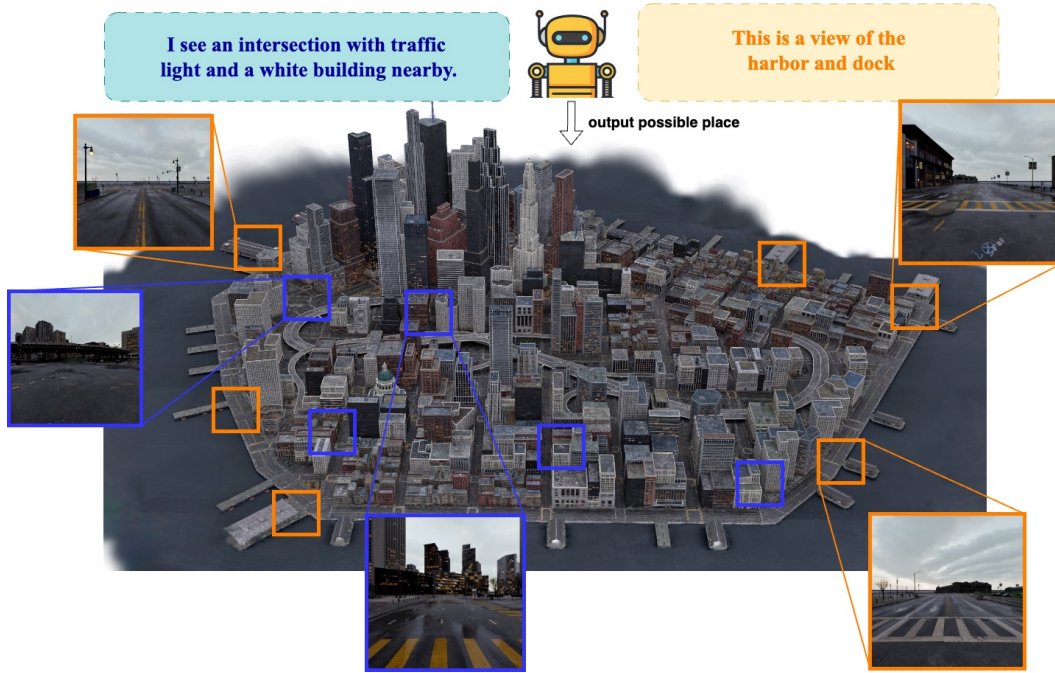


Figure 1. **CityLoc**: Given an ambiguous text description, our method accurately localizes camera poses distribution in the large-scale city, mapping out the likely locations of descriptions like intersections, traffic lights, and urban areas.

## Abstract

Localizing text descriptions in large-scale 3D scenes is inherently an ambiguous task. This nonetheless arises while describing general concepts, e.g. all traffic lights in a city. To facilitate reasoning based on such concepts, text localization in the form of distribution is required. In this paper, we generate the distribution of the camera poses conditioned upon the textual description. To facilitate such generation, we propose a diffusion-based architecture that conditionally diffuses the noisy 6DoF camera poses to their plausible locations. The conditional signals are derived from the text descriptions, using the pre-trained text encoders. The connection between text descriptions and pose distribution is established through

pretrained Vision-Language-Model, i.e. CLIP. Furthermore, we demonstrate that the candidate poses for the distribution can be further refined by rendering potential poses using 3D Gaussian splatting, guiding incorrectly posed samples towards locations that better align with the textual description, through visual reasoning. We demonstrate the effectiveness of our method by comparing it with both standard retrieval methods and learning-based approaches. Our proposed method consistently outperforms these baselines across all five large-scale datasets. Our source code and dataset will be made publicly available.

## 1. Introduction

With the emergence of multi-modal understanding at scale, text and vision inputs are more coupled than ever. They are known to be complimentary, but yet not be available jointly at all times. Therefore, methods such as

✉ Corresponding author: Bin Ren, bin.ren@insait.ai

CLIP [45], DALLE [46], LLaVA [34], and others [1, 4, 9, 10, 26, 30, 43, 59, 73], learn to translate one to the other for several tasks. We are interested in performing localization in a visual environment, i.e. the visual representation of the environment is known, by merely using its text description. Our motivation for doing so comes in twofold: (i) To understand the visual locations based on the language description by humans for natural Human-robot interactions; (ii) To facilitate large-language models (LLMs) to explore the visual scenes through language tokens. We are interested in performing text-based 6 degrees-of-freedom (6DoF) localization at large scenes which are infeasible to be processed in a simple feed-forward manner within the practical means.

The text-based 6DoF localization – at the scale of the large 3D scenes and within the aforementioned motivations – is essentially an ambiguous task in most scenarios. For example, there are many scenarios of “*building next to the street near a traffic light and zebra crossings*”. Therefore, we wish to perform localization covering all possible cases related to the given text description to be localized. More precisely, we wish to generate the distribution of camera poses conditioned upon the textual description. For this, we propose to use the diffusion-based conditional distribution learning technique, where the pose samples of the target distribution are obtained by iteratively updating the noisy poses, while conditioning upon the text features. This differentiates our method from those in [22, 62], which focus on finding the most likely pose and require highly detailed text descriptions.

For the visual representation, we use multiple large-scale 3D Gaussian scenes as shown in Fig. 2, which we built in-house using a recent hierarchical 3D Gaussian method [21]. This representation allows us to rasterize 2D images given 6DoF poses, thus allowing us to perform visual reasoning using images on the pose proposals obtained from the diffusion models. If necessary, the diffusion process itself could potentially be conditioned on the rasterized 2D images to better guide the localization process [58]. However, for the sake of efficiency – since we perform localization at the city scale – we avoid such conditioning. Instead, we utilize the visual 3D representation to further process the pose candidate obtained from the diffusion process. More precisely, the candidate poses generated by conditioning on the input text descriptions are further processed in two phases using the respective rasterized 2D images: (i) a direct filtration of the candidates and (ii) pose refinement through the optimization process, based on the similar between the input text and text description of the rasterized 2D images. Furthermore, we showcase the benefit of the proposed method for the task at hand in the presence of 2D images, as well both image and text in the multi-modal setting.

Our method significantly differs from the closest related works: PoseDiffusion [58] and Text2Pose [22],

Text2Loc [62], and RET [57]. PoseDiffusion localizes the central object, whose poses in the general settings are deterministic and less ambiguous, unlike that of the text description. Furthermore, PoseDiffusion is tailored to perform multi-view bundle adjustment averaging the diffusion process and the iterative rasterization, making it not suitable for large scale localization. Note that the likelihood of finding visually similar images through rasterization decreases exponentially with the increase of the scene’s scale. On the other hand, Text2Pose, Text2Loc, and RET make the assumption that the input description is sufficient to be uniquely localized. They perform localization in 2D which hinders the possibility of visual reasoning through rasterization in our setting. In addition, they are retrieval-based and exploit the point cloud-based scene representation. In our experiments, we show that the retrieval-based solution performs poorly due to the diversity in the scene, limited textual hints, and our requirement of the 6DoF pose parameters.

We apply our method across five different large-scale scenes, covering various viewpoints such as street-level and aerial views. These scenes include diverse environments, from urban to suburban areas, in both real and simulated settings, with a total area exceeding 10 square kilometers. We use Llava [34] to ensure a high diversity of text descriptions during training. During testing, we evaluate performance across different levels of text description granularity, showing that our method achieves better localization accuracy with higher granularity descriptions.

- **Experimental Setup and Benchmarking:** We develop a comprehensive experimental setup designed to evaluate city-scale, text-based 6DoF localization.
- **Novel Approach for Text-Based 6DoF Localization:** We propose a diffusion-based method for text-based 6DoF localization that operates effectively at the city scale.
- **Pose Refinement Technique:** We employ Gaussian splatting rendering for pose refinement, filtering out poorly matched poses and optimizing them by maximizing cosine similarity with text features. This guides the pose to the most relevant location for the given text description.
- **State-of-the-Art Results:** Our approach delivers superior performance, surpassing baseline methods in both pose estimation accuracy and distribution modeling.

## 2. Related Work

**Diffusion Model.** Diffusion models [13, 14, 51], inspired by non-equilibrium thermodynamics, approximate complex data distributions by reversing a noise addition process through a series of diffusion steps. Originally developed for generative tasks, these models have demonstrated impressive results in image [13, 14, 52, 60], video [15, 50], and 3D point cloud generation [32, 39, 47, 70], as well as in natural language [3, 28] and audio generation [44]. More recently, diffusion models have been adapted for discriminative tasks,



Figure 2. We present qualitative results of our large-scale Gaussian splats, including the number of images and the trained Gaussian memory size for each scene.

including image segmentation [2, 7] and visual grounding. However, there has been little exploration of applying diffusion models to camera localization tasks. In this work, we leverage the iterative nature of diffusion to refine probabilistic spatial representations for accurate camera pose estimation. By modeling spatial correlations through a Gaussian representation, we progressively refine the 6 DoF camera pose, achieving high precision and robustness in large-scale scenes, thus showcasing the flexibility of diffusion models in localization and scene understanding.

**Multi-Modal Large Language Models.** To extend the advancements of language models [8, 11, 16, 24, 55] across modalities, Multi-Modal Large Language Models (MLLMs) integrate language and vision [1, 36, 66, 71, 72]. These models excel in tasks requiring an understanding of both text and images, which is relevant for camera localization in large-scale scenes. Flamingo [1] was among the first to align image-text pairs using gated cross-attention blocks, highlighting the importance of multi-modal integration. In 6 DoF camera localization, MLLMs enhance the interpretation of complex urban environments by integrating semantic information from both modalities. End-to-end MLLMs often fine-tune intermediate networks [23, 68] or sampler modules [67] to map visual features into the language space, improving scene representations for localization tasks. Models like BLIP-2 [27], MiniGPT-4 [72], and LLaVA [36] bridge modality gaps using querying transformers and two-stage training processes, demonstrating the effectiveness of combining visual and textual data to enhance localization accuracy. Other notable models such as Otter [25], mPLUG-Owl [64], and InstructBLIP [12] offer architectural inspirations. Drawing from these MLLMs, our method utilizes Gaussian representations [20] to improve 6 DoF camera localization in large-scale scenes, enhancing both accuracy and computational efficiency.

**Large-scale 3D Representation and Localization.** Recent advancements in view synthesis, such as NeRFs [5, 6, 41, 42, 61] and 3DGS [20, 21, 37, 38, 40, 63], have

revolutionized 3D scene representation by utilizing differentiable rendering and optimization. While these methods excel at modeling complex scenes, they struggle with large, unbounded 3D spaces. To address this, several methods have scaled 3D representations by dividing scenes into blocks or using multi-level decompositions, such as Mega-NeRF [56], Block-NeRF [54], CityGaussian [37], and hierarchical 3DGS [21].

Localization and mapping are closely linked, with high-quality 3D reconstructions aiding visual localization. Methods like PoseNet [18] predict camera poses but struggle in large environments. Hloc [48] improves large-scale localization by combining structure-from-motion with global features, while iNeRF [65] and iGS [53] invert NeRFs and 3DGS for 6DoF pose estimation. Text-based methods like Text2Pos [57] and Text2Loc [62] generate poses from descriptions, but can suffer from ambiguity. In contrast, our method learns a distribution of poses from text and refines them using a 3DGS map, marking the first work to bridge text descriptions with pose distributions and use Gaussian representations for large-scale pose refinement.

### 3. Proposed Method

**Problem Setting.** We tackle the problem of estimating 6 DoF pose parameters given text features describing a single scene (e.g., captions or descriptions of scene aspects). Formally, given a tuple  $\mathcal{T} = (T^i)_{i=1}^N$  of  $N \in \mathbb{N}$  input text features  $T^i \in \mathbb{R}^d$ , we aim to recover the tuple  $\mathcal{P} = (P^i)_{i=1}^N$  of corresponding pose parameters  $P^i \in \mathbb{SE}(3)$ .

#### 3.1. Preliminaries:

**Diffusion Models.** Diffusion models [14, 51] are a class of likelihood-based generative models that approximate complex data distributions by inverting a diffusion process from data to a simple distribution via noising and denoising. The noising process transforms data samples  $x$  into noise over a sequence of  $T \in \mathbb{N}$  steps. The model is trained to learn the denoising process.

A Denoising Diffusion Probabilistic Model (DDPM) specifies Gaussian noising. For a variance schedule  $\beta_1, \dots, \beta_T$  across  $T$  steps, the noising transitions are defined as follows:

$$q(x_t | x_{t-1}) = \mathcal{N}(x_t; \sqrt{1 - \beta_t}x_{t-1}, \beta_t\mathbb{I}), \quad (1)$$

where  $\mathbb{I}$  is the identity matrix. This schedule ensures  $x_T$  approaches an isotropic Gaussian, *i.e.*,  $q(x_T) \approx \mathcal{N}(\mathbf{0}, \mathbb{I})$ . Setting  $\alpha_t = 1 - \beta_t$  and  $\bar{\alpha}_t = \prod_{i=1}^t \alpha_i$  yields a closed-form solution for directly sampling  $x_t$  given a data point  $x_0$ :

$$x_t \sim q(x_t | x_0) = \mathcal{N}(x_t; \sqrt{\bar{\alpha}_t}x_0, (1 - \bar{\alpha}_t)\mathbb{I}). \quad (2)$$

For sufficiently small  $\beta_t$ , the reverse  $p_\theta(x_{t-1} | x_t)$  is Gaussian. Thus, we approximate it with model  $\mathcal{F}_\theta$ :

$$p_\theta(x_{t-1} | x_t) = \mathcal{N}(x_{t-1}; \sqrt{\alpha_t}\mathcal{F}_\theta(x_t, t), (1 - \alpha_t)\mathbb{I}). \quad (3)$$

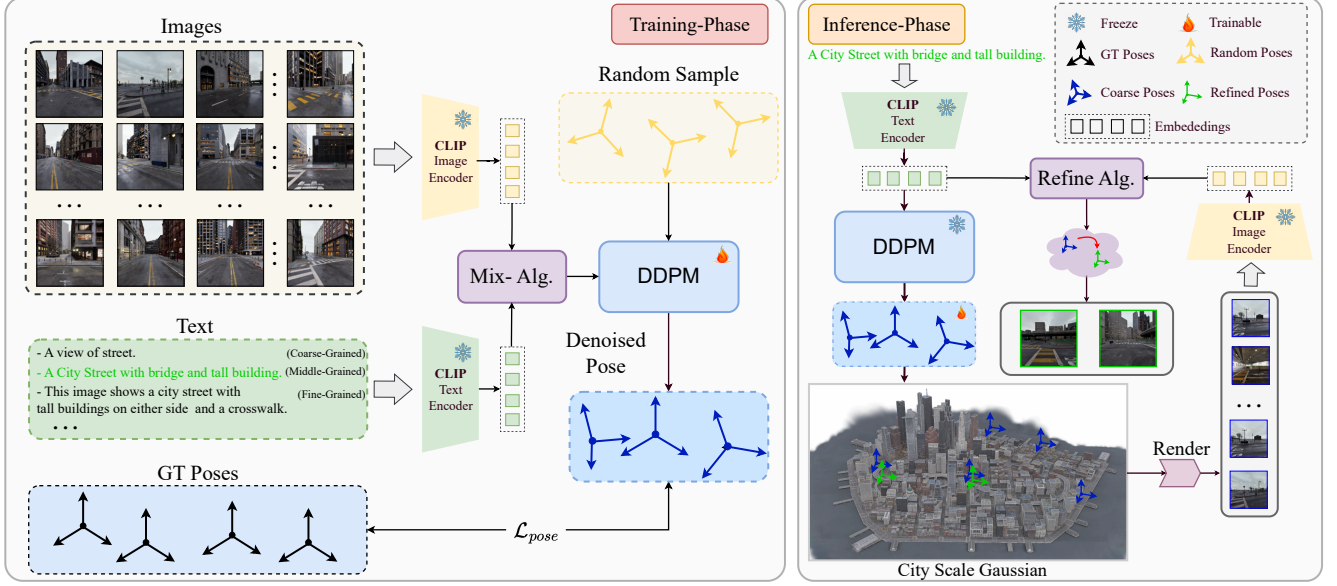


Figure 3. **Overview of CityLoc.** The left panel shows the training process, where images and multi-level of granularity text input are first converted to CLIP features. A fusion algorithm combines these features to train a pose diffusion model, mapping them to a 6DoF camera pose distribution. The right panel illustrates the inference phase, where the pose diffusion model outputs camera poses for any given text input. A pretrained Gaussian field is used to refine the poses, aligning the input text features with the rendered image features.

**3D Gaussian Splatting.** 3DGS represents scene space with Gaussian primitives  $\{Y_i\}_{i=1}^N$ , stacking these as follows:

$$Y = [C, O, S, R, SH] \in \mathbb{R}^{N \times 59}, \quad (4)$$

where  $C \in \mathbb{R}^{N \times 3}$  denotes the centroid,  $O \in \mathbb{R}^{N \times 1}$  the opacity,  $S \in \mathbb{R}^{N \times 3}$  the scale,  $R \in \mathbb{R}^{N \times 4}$  the quaternion rotation vector, and  $SH \in \mathbb{R}^{N \times 48}$  the spherical harmonics. These are collectively termed Gaussian parameters. Each Gaussian softly represents a spatial area with opacity. A point  $q$  in the scene space is influenced by a Gaussian  $Y_i$  according to the Gaussian distribution, weighted by opacity:

$$h_i(q) = O_i \exp\left(-\frac{1}{2}(q - C_i)^T \Sigma_i^{-1}(q - C_i)\right), \quad (5)$$

where covariance  $\Sigma_i$  is formulated as  $\Sigma_i = R_i S_i S_i^T R_i^T$ .

Projected onto a 2D image plane, each Gaussian's influence,  $h$ , contributes to a pixel's color through an alpha-blending equation over the set  $\mathcal{G}$  of influencing Gaussians:

$$c_{\text{pixel}} = \sum_{i \in \mathcal{G}} c_i h_i^{2D} \prod_{j=1}^{i-1} (1 - h_j^{2D}). \quad (6)$$

Through differentiable rasterization, rendering losses are back-propagated to update the Gaussian parameters. In this manner, we represent images rendered from pose  $P$  given by  $I = \mathcal{G}(P)$ .

### 3.2. Text-based Localization

CityLoc models the conditional probability distribution  $p(P|\mathcal{T})$  of pose parameters  $P$  given text features  $\mathcal{T}$ .

Using a diffusion-based model [51, 58], we model  $p(P|\mathcal{T})$  with a denoising process. Specifically,  $p(P|\mathcal{T})$  is estimated by training a diffusion model  $\mathcal{F}_\theta$  on a training set  $\mathcal{S} = \{(P_j, \mathcal{T}_j)\}_{j=1}^M$  of  $M \in \mathbb{N}$  locations with ground truth text features  $\mathcal{T}_j$  and pose parameters  $c_j$ . At inference, for a new set of features  $\mathcal{T}$ , we sample  $p(P|\mathcal{T})$  to estimate pose parameters  $P$ . The denoising process is conditioned on  $\mathcal{T}$ , i.e.,  $p_\theta(P_{t-1} | P_t, \mathcal{T})$ :

$$p_\theta(P_{t-1} | P_t, \mathcal{T}) = \mathcal{N}(P_{t-1}; \sqrt{\alpha_t} \mathcal{F}_\theta(P_t, t, \mathcal{T}), (1 - \alpha_t) \mathbb{I}). \quad (7)$$

**Denoisier  $\mathcal{F}_\theta$ .** The denoisier  $\mathcal{F}_\theta$  is implemented as a Transformer:

$$\mathcal{F}_\theta(P_t, t, \mathcal{T}) = \text{Trans} \left[ \left( \text{cat}(P_t^i, t, \psi(T^i))_{i=1}^N \right) \right] = \mu_{t-1}. \quad (8)$$

Here, the Transformer processes a sequence of noisy tuples  $P_t^i$ , time  $t$ , and embeddings  $\psi(T^i) \in \mathbb{R}^{D_\psi}$  of text features  $T^i$ , outputting the corresponding denoised parameters  $\mu_{t-1} = (\mu_{t-1}^i)_{i=1}^N$ . Training  $\mathcal{F}_\theta$  is supervised by the denoising loss:

$$\mathcal{L}_{\text{diff}} = E_{t \sim [1, T], P_t \sim q(P_t | P_0, \mathcal{T})} \|\mathcal{F}_\theta(P_t, t, \mathcal{T}) - P_0\|^2, \quad (9)$$

where the expectation aggregates over all diffusion steps  $t$ , the diffused samples  $P_t \sim q(P_t | P_0, \mathcal{T})$ , and a training set  $\mathcal{S} = \{(P_{0,j}, \mathcal{T}_j)\}_{j=1}^M$  of scenes with text features  $\mathcal{T}_j$  and poses  $P_{0,j}$ . Following DDPM sampling [14], we initialize with random parameters  $P_T \sim \mathcal{N}(\mathbf{0}, \mathbb{I})$  and, at each iteration

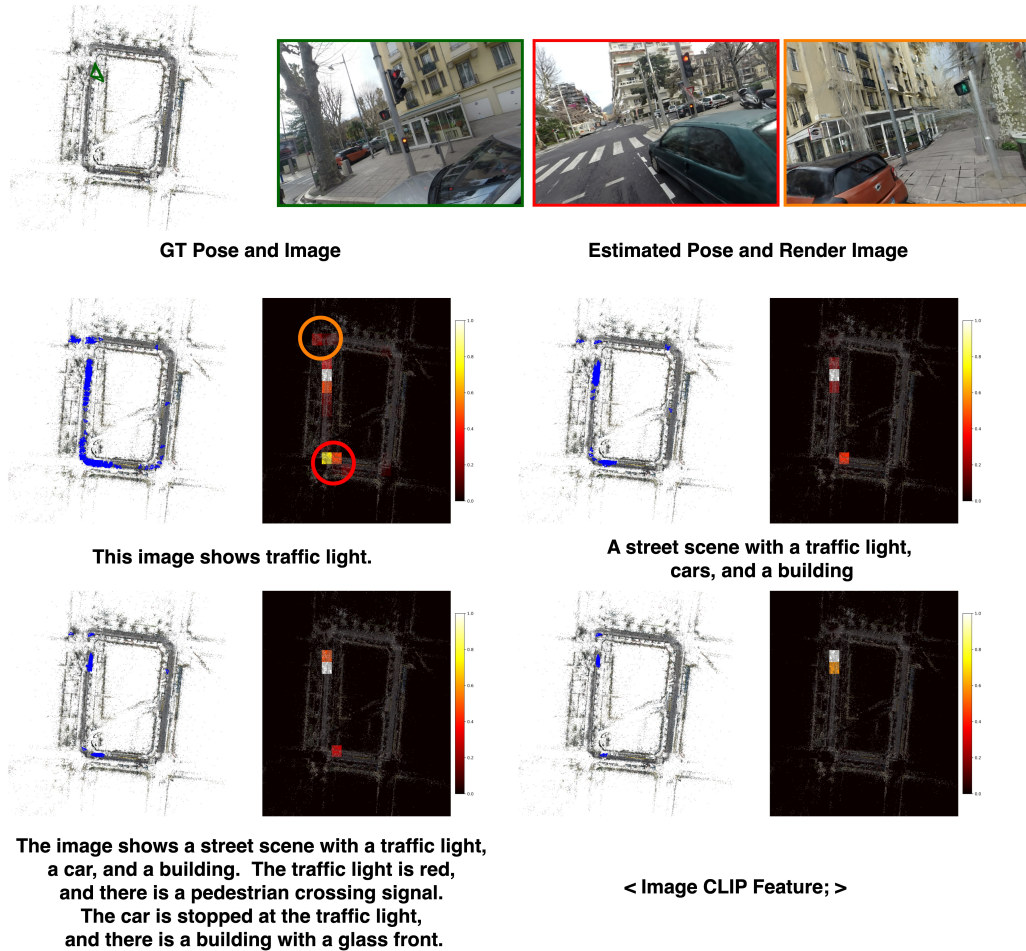


Figure 4. **Qualitative results on the small town dataset:** The enlarged **green camera** and its corresponding images represent those used to generate multiple text prompts with varying levels of granularity. We report the pose distribution conditioned on different levels of text details. The results clearly demonstrate that more informative text inputs lead to more precise location estimates. Additionally, cameras estimated in other locations provide meaningful insights. This is illustrated by selecting a pose within a high-density area as shown in **red camera** and **orange camera**, where both estimates reveal the presence of a traffic light. Zoom in for better visual results.

$t \in (T, \dots, 0)$ , sample the next step  $c_{t-1}$  as:

$$P_{t-1} \sim \mathcal{N}(P_{t-1}; \sqrt{\bar{\alpha}_{t-1}} \mathcal{F}_\theta(P_t, t, \mathcal{T}), (1 - \bar{\alpha}_{t-1}) \mathbb{I}). \quad (10)$$

### 3.3. Text and Gaussian based Refinement

We begin with an initial Gaussian pose estimate  $\hat{P}$ , obtained via a diffusion process, which serves as a probabilistic starting point for our pose configuration. From this initial estimate, we render an image  $\hat{I} = \mathcal{G}(\hat{P})$  using our generator  $\mathcal{G}$ . At the same time, we extract the text feature  $T^i$  directly from the input text through the CLIP text encoder, capturing the semantic richness and intent embedded within the description. Our ultimate goal is to refine the pose  $P$  so that it aligns the generated image with the semantics of the text in a shared feature space, seamlessly bridging visual and linguistic modalities.

To achieve this, we formulate an optimization objective

that minimizes the discrepancy between the text feature  $T$  and the image feature  $\psi_I(G(P))$ , where  $\psi_I$  is the CLIP image encoder. This is expressed as:

$$\min_P \|T - \psi_I(G(P))\|. \quad (11)$$

Initialized with  $\hat{P}$  from the diffusion process,  $P$  is iteratively optimized to reduce this feature distance, driving the pose towards an expressive configuration that captures the nuanced intent of the text. This refinement process not only enhances the coherence between text and image but ensures that the final pose authentically embodies the descriptive depth of the input text, resulting in a highly aligned, semantically resonant image.

### 3.4. The overall Pipeline of the proposed CityLoc

The CityLoc pipeline, illustrated in Fig. 3, integrates both training and inference phases to achieve accurate pose esti-

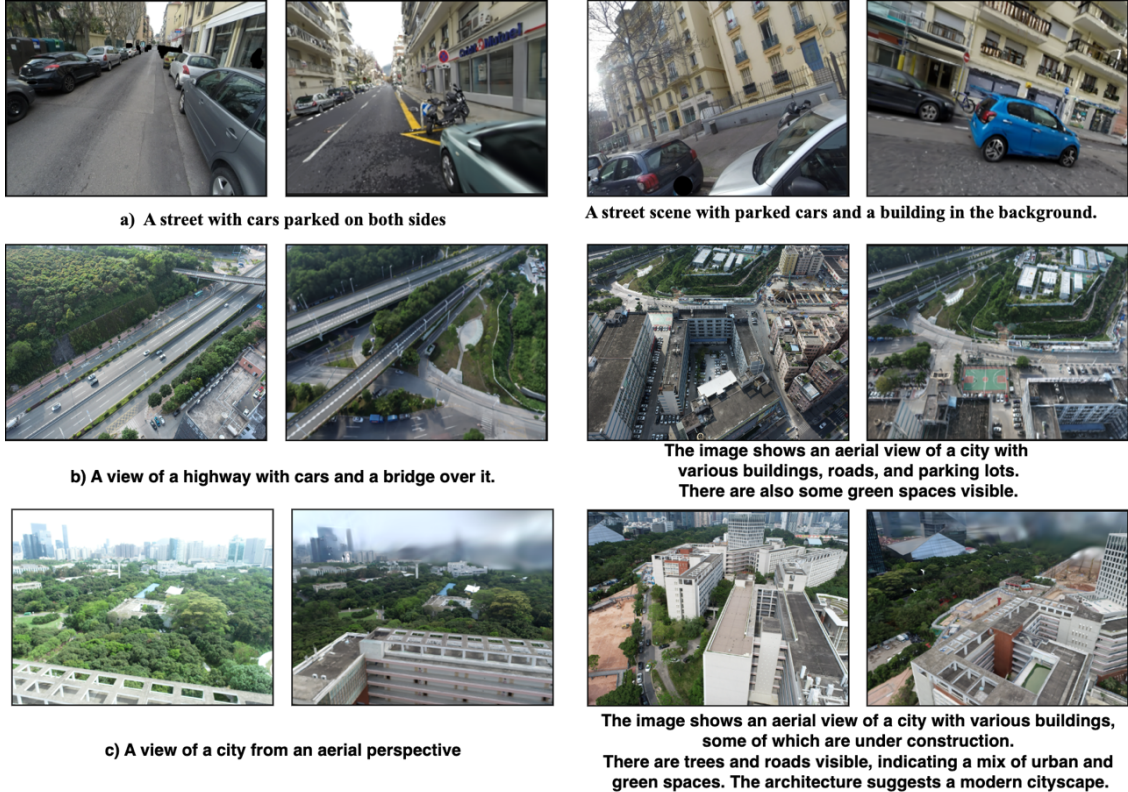


Figure 5. Qualitative results of the proposed method: Training images are shown on the left, with the rendered images on the right.

mation from text prompts. During training, images are processed through the CLIP image encoder and text through the CLIP text encoder, merging their embeddings with a novel mixing algorithm to form a unified representation. These image embeddings condition a diffusion model, which generates denoised pose estimates, optimized by minimizing the discrepancy with known poses. In inference, a text prompt alone is encoded and passed through the pretrained diffusion model to predict poses. These are used with city-scale Gaussian data to render initial images, though biases often arise in these renders. To refine accuracy, we align the rendered image embeddings with those from the original text, iteratively adjusting the poses to eliminate discrepancies. This refinement enables CityLoc to achieve precise, text-aligned pose predictions that faithfully reflect the intended spatial configurations.

## 4. Experiments

### 4.1. Experimental Settings

We evaluate the performance of CityLoc on a diverse set of datasets. First, we assess our method on the Small Town dataset [21], a large-scale collection comprising 5,822 images covering an area of over 40,000 m<sup>2</sup>, with camera poses extracted using COLMAP [49]. Additionally, we test our approach on the UrbanScene3D dataset [31], which contains

high-resolution drone imagery of expansive urban environments. The initial GPS-derived camera poses are refined through a data preprocessing procedure based on MegaNeRF [56]. Finally, we evaluate CityLoc on the extensive MatrixCity dataset [29], which includes 67,000 aerial images and 452,000 street-level images spanning two city maps with a total area of 28 km<sup>2</sup>.

**Text-Prompt Generation.** In constructing the datasets for image captioning, we utilize the LLaVA-NEXT model [33–35] to process images at varying granularities. The text generation is conditioned on a question argument that specifies the desired level of detail in the captions, as outlined below:

- **Nouns:** Generates a list of up to ten nouns that capture the primary visual elements present in the image.
- **Long Sentence:** Produces a detailed caption composed of three concise sentences, providing a comprehensive description of the image.
- **Mid Sentence:** Delivers a balanced description in two sentences, offering an optimal trade-off between detail and conciseness.
- **Short Sentence:** Condenses the image content into a single succinct sentence, emphasizing the most prominent features.

In our experimental framework, the granularity of the

Table 1. We compare performance across five datasets using deep learning-based methods. 1) The regression method follows the approach in [19], with the addition of CLIP embeddings as input. We extend this regression method to distribution learning by incorporating techniques from [17]. 2) The retrieval method uses the nearest K samples to generate a sufficient number of samples close to the text CLIP embedding. 3) For our method, we first report results trained solely on image CLIP features. 4) We then present results using text CLIP features through mixed training. 5) Finally, we refine our approach using Gaussian splat rendering and report the resulting improvements.

Method	$k=15$			$k=10$			$k=5$		
	RE	TE	RDA	RE	TE	RDA	RE	TE	RDA
Small Town									
Regression	5.98	5.98	-	5.83	5.87	-	2.34	1.57	-
MCDrop	10.79	11.46	7.72	7.41	7.28	8.69	3.34	3.31	3.07
Retrieval	5.88	5.67	3.67	3.94	3.95	4.27	2.72	2.08	4.8
Ours	9.25	6.21	16.91	6.66	4.65	15.21	3.71	2.57	11.68
Ours Mixed	5.37	4.54	22.62	4.13	3.35	35.33	2.80	1.99	55.35
Ours Refined	5.88	7.18	26.37	4.95	5.09	41.46	3.11	1.45	57.21
Residence									
Regression	10.39	9.78	-	5.31	6.85	-	1.63	2.89	-
MCDrop	9.17	10.49	4.30	6.99	7.08	6.10	3.78	3.54	3.20
Retrieval	1.81	9.52	3.10	1.76	6.73	4.37	1.49	3.47	2.76
Ours	5.32	10.24	6.23	3.89	7.14	14.01	2.71	3.93	25.83
Ours Mixed	1.58	8.42	10.21	1.56	6.15	20.26	1.47	3.45	25.93
Ours Refined	2.20	8.02	12.42	1.85	6.87	24.21	1.84	3.23	28.85
Sciart									
Regression	9.32	5.38	-	4.96	3.86	-	2.77	2.59	-
MCDrop	10.99	10.79	6.29	7.67	7.62	4.46	3.76	3.63	0.09
Retrieval	7.69	7.91	4.86	5.26	4.82	4.86	2.82	2.44	2.57
Ours	10.75	9.38	19.6	7.29	6.6	28.32	3.63	3.57	27.82
Ours Mixed	7.64	6.48	32.01	5.43	4.30	43.61	3.03	2.58	36.47
Ours Refined	7.76	6.08	34.69	5.95	5.18	44.39	2.68	3.09	39.92
MatrixCity-Street									
Regression	4.99	9.27	-	2.96	5.91	-	1.51	3.30	-
MCDrop	10.07	9.89	1.26	7.13	7.10	1.98	2.63	2.98	2.45
Retrieval	1.74	8.68	1.89	0.87	5.61	2.13	0.49	2.46	2.77
Ours	2.07	9.31	16.44	1.33	6.48	29.86	0.90	3.10	76.46
Ours Mixed	1.74	8.13	7.96	0.99	5.73	12.76	0.64	2.69	27.57
Ours Refined	1.64	8.10	15.11	1.02	5.23	23.24	0.61	2.45	35.21
MatrixCity-Aerial									
Regression	10.07	9.89	1.26	7.13	7.10	1.98	2.63	2.98	2.45
MCDrop	6.14	10.04	0.27	4.24	6.70	0.25	2.27	3.38	0.20
Retrieval	1.47	8.3	2.27	0.57	5.89	4.1	0.46	3.46	3.28
Ours	3.74	9.79	10.50	2.03	6.81	19.9	1.38	3.60	47.13
Ours Mixed	1.82	7.81	9.69	0.87	5.56	18.18	0.61	3.24	35.51
Ours fine	1.94	6.92	13.21	0.92	5.23	20.03	0.67	3.43	39.22

image descriptions varies according to the following levels: in low-granularity experiments, only the list of nouns is used as the image description. For high-granularity experiments, all sentence types are employed, providing a richer textual representation of the image. In the maximum granularity setting, we combine both the noun list and all sentence types to generate the most detailed image description.

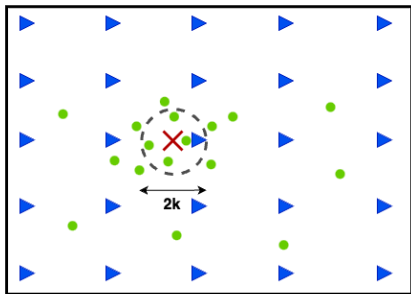
**Evaluation Metrics.** As illustrated in the 2D example in Fig. 6, we evaluate pose estimation using Rotation Error (RE) and Translation Error (TE). We additionally report Relative Distribution Accuracy (RDA) to assess distribution

learning performance. Unlike prior work ([57], [62]), in our task, the ambiguous text input and large-scale scene make it challenging to identify all other positive samples.

**Implementation Details.** All experiments were conducted using an NVIDIA A6000 GPU. We implemented DDPM with an 8-layer transformer. For pose representation, we used a quaternion vector for rotation and a translation vector in global coordinates. The training was done with a learning rate of  $1 \times 10^{-4}$  and a CosineWarmup scheduler. We used the Adam optimizer and trained for 5,000 epochs on most datasets, while for Matrix City Street, was 2,500 epochs.

Table 2. *Granularity Experiments*. For low granularity, we use the template "This is a view of word" with a maximum of five words. For high granularity, we employ descriptions generated by Llava, ranging from short to longer sentences. For maximum granularity, we use the CLIP embedding of images. In this table, we add more baseline for the fair comparison to demonstrate how different granularity could affect the final results.

Method	Low granularity			High granularity			Max granularity		
	RE	TE	RDA	RE	TE	RDA	RE	TE	RDA
Small Town									
Ours	9.98	7.31	2.73	10.48	6.81	3.70	3.35	1.12	83.75
Ours Mixed	5.94	5.67	5.96	5.54	4.34	18.69	3.34	1.54	80.45
Residence									
Ours	6.15	11.71	1.09	5.81	11.22	1.53	1.38	2.89	35.75
Ours Mixed	1.58	9.48	10.67	1.60	8.8	24.84	1.51	4.1	96.18
Sci-Art									
Ours	11.41	11.01	1.18	11.91	10.03	2.32	5.31	2.54	126.70
Ours Mixed	8.08	7.61	7.97	7.87	6.61	19.89	5.60	2.71	120.61
MatrixCity Street									
Ours	2.33	10.59	1.75	2.16	10.59	1.59	1.02	1.62	105.07
Ours Mixed	1.81	8.83	1.89	1.76	8.39	2.98	1.45	5.22	41.13
MatrixCity Aerial									
Ours	4.03	10.79	2.12	4.44	11.05	1.81	0.78	3.03	61.70
Ours Mixed	1.88	8.86	2.72	1.93	7.99	5.43	1.30	4.13	43.38



$$RDA_k = \frac{4 \times \text{green dots}}{1 \times \text{blue triangles}} \quad TE_k = \frac{1}{4} \sum_{i=1}^4 \| \text{green dot} - \text{red X} \|^2$$

Figure 6. **Relative Distribution Accuracy (RDA)** RDA measures the accuracy of the sample distribution within a specified region, defined by a distance threshold  $k$ . The predicted distribution’s sample number equals the uniform samples. **Translation Error (TE)** quantifies localization error by calculating the average translation error of only those samples that fall within the specified region

**Distribution Learning:** We begin by learning position priors for the diffusion model across each large-scale dataset as shown in Tab. 1. Our results demonstrate that our approach outperforms other baselines in terms of RDA, achieving a high concentration of samples near the ground truth pose, with most poses being highly accurate. On smaller datasets, mixed training enhances performance. However, for larger datasets like Matrix City, mixed training leads to worse results, likely due to the increased ambiguity in text descriptions for large-scale scenes.

Additionally, we validated the effectiveness of the Gaus-

sian splatting-based refinement method. By leveraging text CLIP embeddings and rendering image CLIP embeddings to filter and maximize similarity, we achieved significant improvements in distribution performance across most datasets.

**Granularity Experiment:** We report results for different text granularities, as shown in Tab. 2. Our findings clearly demonstrate that, while outperforming the baseline, the RDA score increases with more detailed text. This indicates that the estimated poses become more concentrated around the ground truth. Furthermore, when using the most detailed image CLIP features, we achieve the highest RDA score, we can also see this in Fig. 5 More ablations about granularity will be shown in the supplementary material.

## 5. Conclusion

We presented a diffusion-based framework for text-based 6DoF localization at the city scale, addressing ambiguity and scalability challenges in large, complex environments. By leveraging 3D Gaussian splatting for efficient pose refinement through text and rendered image similarity optimization, our method achieves superior localization accuracy. Thanks to the Gaussian splatting-based scene representation that allows us to perform the visual reasoning during the refinement step. Applied across diverse large-scale scenes, our approach bridges text and visual understanding, enabling natural human-robot interaction and enhancing multi-modal reasoning in visual environments.



## References

- [1] Jean-Baptiste Alayrac, Jeff Donahue, Pauline Luc, Antoine Miech, Iain Barr, Yana Hasson, Karel Lenc, Arthur Mensch, Katherine Millican, Malcolm Reynolds, et al. Flamingo: a visual language model for few-shot learning. *Advances in neural information processing systems*, 35:23716–23736, 2022.
- [2] Tomer Amit, Eliya Nachmani, Tal Shaharbany, and Lior Wolf. Segdiff: Image segmentation with diffusion probabilistic models. *arXiv preprint arXiv:2112.00390*, 2021.
- [3] Jacob Austin, Daniel D Johnson, Jonathan Ho, Daniel Tarlow, and Rianne van den Berg. Structured denoising diffusion models in discrete state-spaces. In *NeurIPS*, pages 17981–17993, 2021.
- [4] Jinze Bai, Shuai Bai, Shusheng Yang, Shijie Wang, Sinan Tan, Peng Wang, Junyang Lin, Chang Zhou, and Jingren Zhou. Qwen-vl: A frontier large vision-language model with versatile abilities. *arXiv preprint arXiv:2308.12966*, 2023.
- [5] Jonathan T. Barron, Ben Mildenhall, Matthew Tancik, Peter Hedman, Ricardo Martin-Brualla, and Pratul P. Srinivasan. Mip-nerf: A multiscale representation for anti-aliasing neural radiance fields. *ICCV*, 2021.
- [6] Jonathan T. Barron, Ben Mildenhall, Dor Verbin, Pratul P. Srinivasan, and Peter Hedman. Mip-nerf 360: Unbounded anti-aliased neural radiance fields. *CVPR*, 2022.
- [7] Emmanuel Asiedu Brempong, Simon Kornblith, Ting Chen, Niki Parmar, Matthias Minderer, and Mohammad Norouzi. Denoising pretraining for semantic segmentation. In *CVPR*, pages 4175–4186, 2022.
- [8] Tom Brown, Benjamin Mann, Nick Ryder, Melanie Subbiah, Jared D Kaplan, Prafulla Dhariwal, Arvind Neelakantan, Pranav Shyam, Girish Sastry, Amanda Askell, et al. Language models are few-shot learners. *Advances in neural information processing systems*, 33:1877–1901, 2020.
- [9] Keqin Chen, Zhao Zhang, Weili Zeng, Richong Zhang, Feng Zhu, and Rui Zhao. Shikra: Unleashing multimodal llm’s referential dialogue magic. *arXiv preprint arXiv:2306.15195*, 2023.
- [10] Xi Chen, Xiao Wang, Soravit Changpinyo, AJ Piergiovanni, Piotr Padlewski, Daniel Salz, Sebastian Goodman, Adam Grycner, Basil Mustafa, Lucas Beyer, et al. Pali: A jointly-scaled multilingual language-image model. In *ICLR*, 2022.
- [11] Aakanksha Chowdhery, Sharan Narang, Jacob Devlin, Maarten Bosma, Gaurav Mishra, Adam Roberts, Paul Barham, Hyung Won Chung, Charles Sutton, Sebastian Gehrmann, et al. Palm: Scaling language modeling with pathways. *Journal of Machine Learning Research*, 24(240):1–113, 2023.
- [12] Wenliang Dai, Junnan Li, Dongxu Li, Anthony Meng Huat Tiong, Junqi Zhao, Weisheng Wang, Boyang Li, Pascale N Fung, and Steven Hoi. Instructblip: Towards general-purpose vision-language models with instruction tuning. *Advances in Neural Information Processing Systems*, 36, 2024.
- [13] Prafulla Dhariwal and Alexander Nichol. Diffusion models beat gans on image synthesis. In *NeurIPS*, pages 8780–8794, 2021.
- [14] Jonathan Ho, Ajay Jain, and Pieter Abbeel. Denoising diffusion probabilistic models. In *NeurIPS*, pages 6840–6851, 2020.
- [15] Jonathan Ho, Tim Salimans, Alexey Gritsenko, William Chan, Mohammad Norouzi, and David J Fleet. Video diffusion models. *arXiv preprint arXiv:2204.03458*, 2022.
- [16] Jordan Hoffmann, Sebastian Borgeaud, Arthur Mensch, Elena Buchatskaya, Trevor Cai, Eliza Rutherford, Diego de Las Casas, Lisa Anne Hendricks, Johannes Welbl, Aidan Clark, et al. Training compute-optimal large language models. *arXiv preprint arXiv:2203.15556*, 2022.
- [17] Alex Kendall and Roberto Cipolla. Modelling uncertainty in deep learning for camera relocalization, 2016.
- [18] Alex Kendall, Matthew Grimes, and Roberto Cipolla. Posenet: A convolutional network for real-time 6-dof camera relocalization. In *Proceedings of the IEEE international conference on computer vision*, pages 2938–2946, 2015.
- [19] Alex Kendall, Matthew Grimes, and Roberto Cipolla. Posenet: A convolutional network for real-time 6-dof camera relocalization, 2016.
- [20] Bernhard Kerbl, Georgios Kopanas, Thomas Leimkühler, and George Drettakis. 3d gaussian splatting for real-time radiance field rendering. *ACM Trans. Graph.*, 42(4):139–1, 2023.
- [21] Bernhard Kerbl, Andréas Meuleman, Georgios Kopanas, Michael Wimmer, Alexandre Lanvin, and George Drettakis. A hierarchical 3d gaussian representation for real-time rendering of very large datasets, 2024.
- [22] Manuel Kolmet, Qunjie Zhou, Aljoša Ošep, and Laura Leal-Taixé. Text2pos: Text-to-point-cloud cross-modal localization. In *Proceedings of the IEEE/CVF Conference on Computer Vision and Pattern Recognition*, pages 6687–6696, 2022.
- [23] Xin Lai, Zhuotao Tian, Yukang Chen, Yanwei Li, Yuhui Yuan, Shu Liu, and Jiaya Jia. Lisa: Reasoning segmentation via large language model. In *Proceedings of the IEEE/CVF Conference on Computer Vision and Pattern Recognition*, pages 9579–9589, 2024.
- [24] Teven Le Scao, Angela Fan, Christopher Akiki, Ellie Pavlick, Suzana Ilić, Daniel Hesslow, Roman Castagné, Alexandra Sasha Luccioni, François Yvon, Matthias Gallé, et al. Bloom: A 176b-parameter open-access multilingual language model. 2023.
- [25] Bo Li, Yuanhan Zhang, Liangyu Chen, Jinghao Wang, Jingkang Yang, and Ziwei Liu. Otter: A multi-modal model with in-context instruction tuning, 2023.
- [26] Chunyuan Li, Cliff Wong, Sheng Zhang, Naoto Usuyama, Haotian Liu, Jianwei Yang, Tristan Naumann, Hoifung Poon, and Jianfeng Gao. Llava-med: Training a large language-and-vision assistant for biomedicine in one day. *Advances in Neural Information Processing Systems*, 36, 2024.
- [27] Junnan Li, Dongxu Li, Silvio Savarese, and Steven Hoi. Blip-2: Bootstrapping language-image pre-training with frozen image encoders and large language models. In *International conference on machine learning*, pages 19730–19742. PMLR, 2023.
- [28] Xiang Lisa Li, John Thickstun, Ishaan Gulrajani, Percy Liang, and Tatsunori B Hashimoto. Diffusion-lm improves controllable text generation. *arXiv preprint arXiv:2205.14217*, 2022.

- [29] Yixuan Li, Lihan Jiang, Linning Xu, Yuanbo Xiangli, Zhenzhi Wang, Dahua Lin, and Bo Dai. Matrixcity: A large-scale city dataset for city-scale neural rendering and beyond. In *Proceedings of the IEEE/CVF International Conference on Computer Vision*, pages 3205–3215, 2023.
- [30] Bin Lin, Zhenyu Tang, Yang Ye, Jiayi Cui, Bin Zhu, Peng Jin, Jinfa Huang, Junwu Zhang, Yatian Pang, Munan Ning, et al. Moe-llava: Mixture of experts for large vision-language models. *arXiv preprint arXiv:2401.15947*, 2024.
- [31] Liqiang Lin, Yilin Liu, Yue Hu, Xingguang Yan, Ke Xie, and Hui Huang. Capturing, reconstructing, and simulating: the urbanscene3d dataset. In *ECCV*, pages 93–109, 2022.
- [32] Chang Liu, Mengyi Zhao, Bin Ren, Mengyuan Liu, Nicu Sebe, et al. Spatio-temporal graph diffusion for text-driven human motion generation. In *BMVC*, pages 722–729, 2023.
- [33] Haotian Liu, Chunyuan Li, Qingyang Wu, and Yong Jae Lee. Visual instruction tuning, 2023.
- [34] Haotian Liu, Chunyuan Li, Qingyang Wu, and Yong Jae Lee. Visual instruction tuning, 2023.
- [35] Haotian Liu, Chunyuan Li, Yuheng Li, Bo Li, Yuanhan Zhang, Sheng Shen, and Yong Jae Lee. Llava-next: Improved reasoning, ocr, and world knowledge, 2024.
- [36] Haotian Liu, Chunyuan Li, Qingyang Wu, and Yong Jae Lee. Visual instruction tuning. *Advances in neural information processing systems*, 36, 2024.
- [37] Yang Liu, He Guan, Chuanchen Luo, Lue Fan, Junran Peng, and Zhaoxiang Zhang. Citygaussian: Real-time high-quality large-scale scene rendering with gaussians, 2024.
- [38] Haozhe Lou, Yurong Liu, Yike Pan, Yiran Geng, Jianteng Chen, Wenlong Ma, Chenglong Li, Lin Wang, Hengzhen Feng, Lu Shi, et al. Robo-gs: A physics consistent spatial-temporal model for robotic arm with hybrid representation. *arXiv preprint arXiv:2408.14873*, 2024.
- [39] Zhaoyang Lyu, Zhifeng Kong, Xudong Xu, Liang Pan, and Dahua Lin. A conditional point diffusion-refinement paradigm for 3d point cloud completion. *arXiv preprint arXiv:2112.03530*, 2021.
- [40] Qi Ma, Yue Li, Bin Ren, Nicu Sebe, Ender Konukoglu, Theo Gevers, Luc Van Gool, and Danda Pani Paudel. Shapesplat: A large-scale dataset of gaussian splats and their self-supervised pretraining. In *International Conference on 3D Vision*, 2025.
- [41] Ben Mildenhall, Pratul P Srinivasan, Matthew Tancik, Jonathan T Barron, Ravi Ramamoorthi, and Ren Ng. Nerf: Representing scenes as neural radiance fields for view synthesis. *Communications of the ACM*, 65(1):99–106, 2021.
- [42] Thomas Müller, Alex Evans, Christoph Schied, and Alexander Keller. Instant neural graphics primitives with a multiresolution hash encoding. *ACM Trans. Graph.*, 41(4):102:1–102:15, 2022.
- [43] Zhiliang Peng, Wenhui Wang, Li Dong, Yaru Hao, Shaohan Huang, Shuming Ma, and Furu Wei. Kosmos-2: Grounding multimodal large language models to the world. *arXiv preprint arXiv:2306.14824*, 2023.
- [44] Vadim Popov, Ivan Vovk, Vladimir Gogoryan, Tasnima Sadekova, and Mikhail Kudinov. Grad-tts: A diffusion probabilistic model for text-to-speech. In *ICML*, pages 8599–8608, 2021.
- [45] Alec Radford, Jong Wook Kim, Chris Hallacy, Aditya Ramesh, Gabriel Goh, Sandhini Agarwal, Girish Sastry, Amanda Askell, Pamela Mishkin, Jack Clark, Gretchen Krueger, and Ilya Sutskever. Learning transferable visual models from natural language supervision, 2021.
- [46] Aditya Ramesh, Mikhail Pavlov, Gabriel Goh, Scott Gray, Chelsea Voss, Alec Radford, Mark Chen, and Ilya Sutskever. Zero-shot text-to-image generation, 2021.
- [47] Bin Ren, Mengyuan Liu, Runwei Ding, and Hong Liu. A survey on 3d skeleton-based action recognition using learning method. *Cyborg and Bionic Systems*, 5:0100, 2024.
- [48] Paul-Edouard Sarlin, Cesar Cadena, Roland Siegwart, and Marcin Dymczyk. From coarse to fine: Robust hierarchical localization at large scale. In *CVPR*, 2019.
- [49] Johannes Lutz Schönberger and Jan-Michael Frahm. Structure-from-Motion Revisited. In *Conference on Computer Vision and Pattern Recognition (CVPR)*, 2016.
- [50] Uriel Singer, Adam Polyak, Thomas Hayes, Xi Yin, Jie An, Songyang Zhang, Qiyuan Hu, Harry Yang, Oron Ashual, Oran Gafni, et al. Make-a-video: Text-to-video generation without text-video data. *arXiv preprint arXiv:2209.14792*, 2022.
- [51] Jascha Sohl-Dickstein, Eric Weiss, Niru Maheswaranathan, and Surya Ganguli. Deep unsupervised learning using nonequilibrium thermodynamics. In *ICML*, pages 2256–2265, 2015.
- [52] Jiaming Song, Chenlin Meng, and Stefano Ermon. Denoising diffusion implicit models. *arXiv preprint arXiv:2010.02502*, 2020.
- [53] Yuan Sun, Xuan Wang, Yunfan Zhang, Jie Zhang, Caigui Jiang, Yu Guo, and Fei Wang. icomma: Inverting 3d gaussians splatting for camera pose estimation via comparing and matching. *arXiv preprint arXiv:2312.09031*, 2023.
- [54] Matthew Tancik, Vincent Casser, Xinchen Yan, Sabeek Pradhan, Ben Mildenhall, Pratul P Srinivasan, Jonathan T Barron, and Henrik Kretzschmar. Block-nerf: Scalable large scene neural view synthesis. In *Proceedings of the IEEE/CVF Conference on Computer Vision and Pattern Recognition*, pages 8248–8258, 2022.
- [55] Hugo Touvron, Thibaut Lavril, Gautier Izacard, Xavier Martinet, Marie-Anne Lachaux, Timothée Lacroix, Baptiste Rozière, Naman Goyal, Eric Hambro, Faisal Azhar, et al. Llama: Open and efficient foundation language models. *arXiv preprint arXiv:2302.13971*, 2023.
- [56] Haithem Turki, Deva Ramanan, and Mahadev Satyanarayanan. Mega-nerf: Scalable construction of large-scale nerfs for virtual fly-throughs. In *Proceedings of the IEEE/CVF Conference on Computer Vision and Pattern Recognition*, pages 12922–12931, 2022.
- [57] Guangzhi Wang, Hehe Fan, and Mohan Kankanhalli. Text to point cloud localization with relation-enhanced transformer. In *Proceedings of the AAAI Conference on Artificial Intelligence*, pages 2501–2509, 2023.
- [58] Jianyuan Wang, Christian Rupprecht, and David Novotny. Posediffusion: Solving pose estimation via diffusion-aided bundle adjustment. In *Proceedings of the IEEE/CVF International Conference on Computer Vision*, pages 9773–9783, 2023.

- [59] Wenhai Wang, Zhe Chen, Xiaokang Chen, Jiannan Wu, Xizhou Zhu, Gang Zeng, Ping Luo, Tong Lu, Jie Zhou, Yu Qiao, et al. Visionllm: Large language model is also an open-ended decoder for vision-centric tasks. *NeurIPS*, 2023.
- [60] Yinhuai Wang, Jiwen Yu, and Jian Zhang. Zero-shot image restoration using denoising diffusion null-space model. In *ICLR*, 2022.
- [61] Zirui Wu, Tianyu Liu, Liyi Luo, Zhidong Zhong, Jianteng Chen, Hongmin Xiao, Chao Hou, Haozhe Lou, Yuantao Chen, Runyi Yang, et al. Mars: An instance-aware, modular and realistic simulator for autonomous driving. In *CAAI International Conference on Artificial Intelligence*, pages 3–15. Springer, 2023.
- [62] Yan Xia, Letian Shi, Zifeng Ding, Joao F Henriques, and Daniel Cremers. Text2loc: 3d point cloud localization from natural language. In *Proceedings of the IEEE/CVF Conference on Computer Vision and Pattern Recognition*, pages 14958–14967, 2024.
- [63] Runyi Yang, Zhenxin Zhu, Zhou Jiang, Baijun Ye, Xiaoxue Chen, Yifei Zhang, Yuantao Chen, Jian Zhao, and Hao Zhao. Spectrally pruned gaussian fields with neural compensation. *arXiv preprint arXiv:2405.00676*, 2024.
- [64] Qinghao Ye, Haiyang Xu, Guohai Xu, Jiabo Ye, Ming Yan, Yiyang Zhou, Junyang Wang, Anwen Hu, Pengcheng Shi, Yaya Shi, et al. mplug-owl: Modularization empowers large language models with multimodality. *arXiv preprint arXiv:2304.14178*, 2023.
- [65] Lin Yen-Chen, Pete Florence, Jonathan T Barron, Alberto Rodriguez, Phillip Isola, and Tsung-Yi Lin. inerf: Inverting neural radiance fields for pose estimation. In *2021 IEEE/RSJ International Conference on Intelligent Robots and Systems (IROS)*, pages 1323–1330. IEEE, 2021.
- [66] Shukang Yin, Chaoyou Fu, Sirui Zhao, Ke Li, Xing Sun, Tong Xu, and Enhong Chen. A survey on multimodal large language models. *arXiv preprint arXiv:2306.13549*, 2023.
- [67] Haoxuan You, Haotian Zhang, Zhe Gan, Xianzhi Du, Bowen Zhang, Zirui Wang, Liangliang Cao, Shih-Fu Chang, and Yinfei Yang. Ferret: Refer and ground anything anywhere at any granularity. *arXiv preprint arXiv:2310.07704*, 2023.
- [68] Ao Zhang, Liming Zhao, Chen-Wei Xie, Yun Zheng, Wei Ji, and Tat-Seng Chua. Next-chat: An lmm for chat, detection and segmentation. *arXiv preprint arXiv:2311.04498*, 2023.
- [69] Beichen Zhang, Pan Zhang, Xiaoyi Dong, Yuhang Zang, and Jiaqi Wang. Long-clip: Unlocking the long-text capability of clip. In *European Conference on Computer Vision*, pages 310–325. Springer, 2025.
- [70] Mengyi Zhao, Mengyuan Liu, Bin Ren, Shuling Dai, and Nicu Sebe. Denoising diffusion probabilistic models for action-conditioned 3d motion generation. In *ICASSP 2024-2024 IEEE International Conference on Acoustics, Speech and Signal Processing (ICASSP)*, pages 4225–4229. IEEE, 2024.
- [71] Yuhang Zheng, Xiangyu Chen, Yupeng Zheng, Songen Gu, Runyi Yang, Bu Jin, Pengfei Li, Chengliang Zhong, Zengmao Wang, Lina Liu, et al. Gaussiangrasper: 3d language gaussian splatting for open-vocabulary robotic grasping. *arXiv preprint arXiv:2403.09637*, 2024.
- [72] Deyao Zhu, Jun Chen, Xiaoqian Shen, Xiang Li, and Mohamed Elhoseiny. Minigt-4: Enhancing vision-language understanding with advanced large language models. *arXiv preprint arXiv:2304.10592*, 2023.
- [73] Deyao Zhu, Jun Chen, Xiaoqian Shen, Xiang Li, and Mohamed Elhoseiny. Minigt-4: Enhancing vision-language understanding with advanced large language models. *arXiv preprint arXiv:2304.10592*, 2023.

# CityLoc: 6 DoF Localization of Text Descriptions in Large-Scale Scenes with Gaussian Representation

## Supplementary Material

In this supplementary material, we provide additional details to enhance the clarity and comprehensiveness of our work. First, we present two important corrections and clarifications in Sec. 1, addressing key points that strengthen our claims. Next, the experimental setups are detailed in Sec. 2, followed by an in-depth analysis of the ablation experiments in Sec. 3, which demonstrate the effectiveness of our approach. Finally, we discuss further implications and insights in Sec. 4 and conclude with an exploration of the broader impact of our work in Sec. 5.

### 1. Corrections

We report two corrections on the main page: 1) In Fig.4 of our main manuscript, the caption has been updated to: Qualitative results of different text granularity in the small town dataset. 2) In Fig.6 of our main manuscript, we add the following clarification: The results are calculated based on a uniform sample number and the generated sample numbers.

### 2. Experimental Setups

**Gaussian Training.** To process large-scale scenes, we utilize H3DGS [21] for Gaussian training. Chunk sizes are set to  $100 \times 100$  for street views and  $200 \times 200$  for aerial views. The datasets are partitioned into the following chunks: 4 for the small town dataset, 2 for the SciArt dataset, 4 for the residence dataset, 66 for the Matrix City aerial dataset, and 203 for the Matrix City small dataset. Each chunk is trained for 60,000 iterations. Subsequently, chunks are merged following hierarchy optimization; however, for the Matrix City dataset, memory constraints as shown in Fig.2 of our main manuscript prevent merging all chunks. Instead, only adjacent chunks are merged with overlap. For each dataset, we first use the training views from regarding dataset to construct the Gaussian splats. Subsequently, we randomly select 10% of the poses as the validation set, while the remaining 90% are used to train the diffusion model.

**Diffusion Model Training.** In addition to the details mentioned in our main manuscript, for each batch, we randomly select 90 different timesteps out of a total of 100. We optimize the noise prediction step-by-step with a dropout rate of 0.1. The beta scheduler follows a linear progression from  $1 \times 10^{-4}$  to 0.1. For optimization, we use an  $L_1$  loss function for both translation and rotation quaternions. For the CLIP model, we use the pretrained laion2bs34b-b88k. For LLava, we utilize the lmms-lab/llama3-llava-next-8b model.

**Mixup Training Algorithm.** To tackle the challenge of text-

---

#### Algorithm 1 Mixup Training Algorithm

---

**Require:**

**Inputs:**

- Image  $\mathbf{I}$  and text  $\mathbf{T}$
- Random pose  $P_{\text{rand}}$  and ground truth pose  $P_{\text{gt}}$
- Swap ratio  $\beta \in [0, 1]$  (hyperparameter)
- Diffusion model  $h_{\text{DDPM}}$
- CLIP Text Encoder (providing  $\mathbf{T}$ ) and CLIP Image Encoder  $f_{\text{CLIP,img}}$

**Ensure:** Refined predicted pose  $P_{\text{pred}}$

- 1: Compute image embedding:  $\mathbf{E}_I \leftarrow f_{\text{CLIP,img}}(\mathbf{I})$
- 2: Compute text embedding:  $\mathbf{E}_T \leftarrow f_{\text{CLIP,text}}(\mathbf{T})$
- 3: Combine embeddings:

$$\mathbf{E}_{\text{mix}} \leftarrow \begin{cases} \mathbf{E}_T & \text{with probability } \beta, \\ \mathbf{E}_I & \text{with probability } 1 - \beta. \end{cases}$$

- 4: Predict pose:  $P_{\text{pred}} \leftarrow h_{\text{DDPM}}(\mathbf{E}_{\text{mix}}, P_{\text{rand}})$
  - 5: Compute loss:  $\mathcal{L} \leftarrow \|P_{\text{pred}} - P_{\text{gt}}\|^2$
  - 6: Update model:  $h_{\text{DDPM}} \leftarrow \arg \min_h \mathbb{E}[\mathcal{L}]$
  - 7: **for** epoch = 1 to N **do**
  - 8:     Repeat from step 1
  - 9: **end for**
  - 10: **return**  $P_{\text{pred}}$
- 

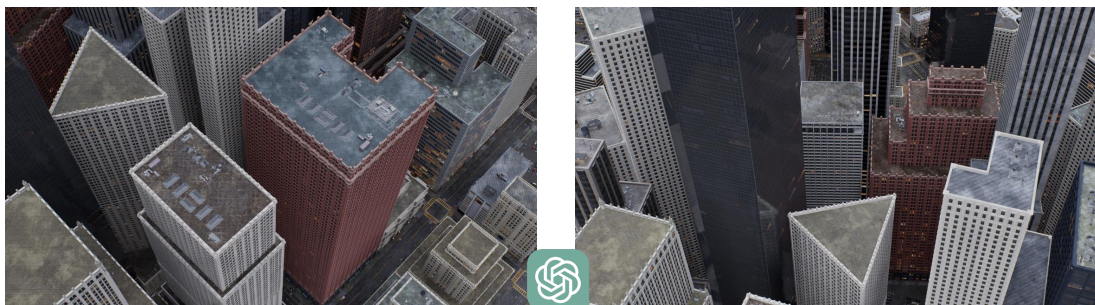
based 6DoF localization at the city scale, where mapping ambiguous textual descriptions to precise camera poses is inherently difficult, we propose the Mixup Training Algorithm (Algorithm 1). This algorithm bridges the gap between input textual descriptions and predicted camera poses by introducing a novel embedding combination strategy during training. First, embeddings are generated for images and texts using a CLIP Image Encoder and a CLIP Text Encoder, respectively. These embeddings are then blended using a learnable swap ratio, which dynamically controls the contribution of text and image features.

To enhance representational capacity, the combined embeddings are further processed through an MLP and used as conditional inputs to a diffusion model (DDPM), which predicts the camera pose. By minimizing the mean squared error between the predicted and ground truth poses, the model is optimized to embed textual information directly into the pose prediction process without sacrificing the spatial precision provided by image data. This approach ensures a robust alignment between text and pose, reduces ambiguity in text-to-pose mapping, and achieves accurate localization

Table A. Ablations about granularity on small town dataset.

Granularity	CLIP Cos	Low granularity			High granularity			Max granularity			Mean		
		RE	TE	RDA	RE	TE	RDA	RE	TE	RDA	RE	TE	RDA
1 noun	0.19	6.39	6.05	3.21	6.94	6.05	4.57	3.35	1.67	81.32	5.56	4.59	29.70
3 nouns	0.25	6.13	5.65	7.30	7.16	6.42	4.86	3.43	1.56	81.38	5.57	4.54	31.18
5 nouns	0.27	6.22	5.57	9.69	6.80	6.00	7.08	3.45	1.48	80.05	5.49	4.35	32.27
All nouns	0.23	5.83	5.45	7.68	6.02	6.03	7.50	3.39	1.58	80.37	5.08	4.35	31.85
short sentence	0.27	6.97	6.96	3.38	6.16	4.20	19.41	3.49	1.45	80.48	5.54	4.20	34.42
middle sentence	0.27	7.14	6.62	3.89	5.85	3.98	23.49	3.40	1.45	81.44	5.46	4.02	36.27
long sentence	0.29	7.45	6.54	3.75	6.08	3.99	26.51	3.39	1.43	80.81	5.64	4.00	37.02
All sentences	0.28	6.61	6.40	3.84	5.43	3.62	27.27	3.37	1.48	80.88	5.14	3.83	37.33
All	0.25	5.94	5.67	5.96	5.54	4.34	18.69	3.34	1.54	80.45	4.94	3.85	35.03

Llava: The image shows a cityscape with tall buildings. The buildings are of various designs and heights. The photo is taken from an aerial perspective.



This image shows a dense cityscape with a reddish-brown building standing out among gray and white skyscrapers, including a triangular-roofed structure in the foreground. Rooftops feature detailed urban infrastructure like vents and HVAC units. The faint streets below add depth to the scene.

This view highlights a towering black skyscraper surrounded by reddish-brown and gray buildings of varied styles. The triangular building reappears, contrasting with the square and rectangular forms around it. Detailed rooftops and visible streets emphasize the urban density.

Figure A. **Limitations on generated text for large scale scene:** We used the Llava model for image captioning at different granularities, but we found that for larger and more complex scenes, the text generated by Llava fails to extract more effective information. For example, as shown in the image above, for two pictures with numerous city buildings, Llava fails to generate distinct text prompts. In contrast, ChatGPT provides very detailed information that is helpful for localization.

Table B. Ablations about swap probability.

Swap Probability	Small Town		
	RE	TE	RDA
0	9.25	6.21	16.91
0.1	7.07	4.99	18.92
0.3	5.78	4.56	21.8
0.5	5.39	4.43	22.99
0.7	<b>5.26</b>	<b>4.33</b>	<b>23.64</b>
0.9	5.28	4.33	22.56
1.0	5.45	4.72	15.28

in large-scale, complex environments.

**Gaussian Refinement Algorithm.** To identify the pose that best matches the text embedding at the feature level from the many possible outputs of a diffusion model, we propose the

Gaussian Refinement Algorithm (Algorithm 2). This algorithm iteratively refines an initial coarse pose by aligning its rendered view with the corresponding textual description in the embedding space, leveraging city-scale Gaussian models and the expressiveness of CLIP embeddings to achieve robust text-to-pose refinement.

The refinement process begins with a coarse camera pose, which is used to render a synthetic view based on the Gaussian model and pipeline parameters. During refinement, we follow the steps outlined in ICOMA, rendering images at a resolution of  $224 \times 224$  while maintaining the same field of view (FoV). For images with differing aspect ratios, the shorter side is resized to 224 pixels, and the longer side is cropped to match the aspect ratio. Since the rasterization process only allows optimization of one image at a time, optimizing across all poses in the test set would be computationally prohibitive. Thus, refinement is conducted on a

---

**Algorithm 2** Gaussian Refinement Algorithm

---

**Require:****Inputs:**

- Initial coarse camera pose  $P_{\text{coarse}}$
- Ground truth pose  $P_{\text{gt}}$
- City-scale Gaussian model  $\mathcal{G}$ , background  $\mathbf{B}$
- Pipeline parameters  $\Phi$
- Hyperparameters: learning rate  $\eta$ , iterations  $N$
- Text features  $\mathbf{T}$  (from CLIP Text Encoder)
- CLIP Image Encoder  $f_{\text{CLIP,img}}$

**Ensure:** Refined camera pose  $P_{\text{refined}}$ , success flag success

```
1: Initialize predicted pose:  $P_{\text{pred}} \leftarrow P_{\text{coarse}}$ 
2: Initialize optimizer: Adam( $P_{\text{pred}}, \eta$ )
3: Compute initial rendering:  $\mathbf{R} \leftarrow$ 
   Render( $P_{\text{pred}}, \mathcal{G}, \Phi, \mathbf{B}$ )
4: Normalize rendering:  $\mathbf{R}_{\text{norm}} \leftarrow f_{\text{CLIP,img}}(\mathbf{R})$ 
5: Compute initial similarity:  $\mathcal{L}_{\text{init}} \leftarrow \mathbf{R}_{\text{norm}} \cdot \mathbf{T}^\top$ 
6: if  $\mathcal{L}_{\text{init}} < \tau_1$  then
7:   return  $P_{\text{pred}}, \text{False}$   $\triangleright$  Reject poor initial pose
8: end if
9: for  $k = 1$  to  $N$  do
10:   $\mathbf{R} \leftarrow$  Render( $P_{\text{pred}}, \mathcal{G}, \Phi, \mathbf{B}$ )
11:   $\mathbf{R}_{\text{norm}} \leftarrow f_{\text{CLIP,img}}(\mathbf{R})$ 
12:   $\mathcal{L}_{\text{clip}} \leftarrow \mathbf{R}_{\text{norm}} \cdot \mathbf{T}^\top$ 
13:  Loss:  $\mathcal{L} \leftarrow -\mathcal{L}_{\text{clip}}$   $\triangleright$  Maximize similarity
14:  Backpropagate:  $\nabla_{P_{\text{pred}}} \mathcal{L}$ 
15:  Update pose:  $P_{\text{pred}} \leftarrow P_{\text{pred}} - \eta \nabla_{P_{\text{pred}}} \mathcal{L}$ 
16: end for
17: if  $\mathcal{L}_{\text{clip}} < \tau_2$  or  $\mathcal{L}_{\text{clip}} - \mathcal{L}_{\text{init}} < \tau_3$  then
18:   return  $P_{\text{pred}}, \text{False}$   $\triangleright$  Reject refinement
19: end if
20: return  $P_{\text{pred}}, \text{True}$ 
```

---

randomly selected 10% subset of the test set. In each refinement iteration, the rendered view is normalized and encoded using a CLIP Image Encoder, generating an embedding that is compared to the text embedding from a CLIP Text Encoder. A similarity score is computed between the two embeddings, and the loss is formulated as the negative of this similarity. Using gradient-based optimization, the coarse pose is iteratively updated to maximize the feature-level alignment with the text embedding. To ensure robustness, the algorithm incorporates rejection mechanisms, discarding poses that fail to meet minimum similarity thresholds. By combining Gaussian models with CLIP embeddings and adhering to computationally efficient refinement steps, the Algorithm 2 effectively bridges the gap between text descriptions and 6DoF camera poses, delivering accurate localization results even in large-scale 3D environments.

### 3. Ablation Experiments

**Ablation on text granularity.** In Tab. A, we perform an ablation study to understand the impact of text granularity on model performance using the small town dataset. The granularity levels are defined as follows:

- **1 noun:** Single noun descriptions (e.g., *tree*”).
- **3 nouns:** Phrases containing three nouns (e.g., *tree, house, car*”).
- **5 nouns:** Phrases containing five nouns (e.g., *tree, house, car, road, lamp*”).
- **All nouns:** All nouns above.
- **Short sentence:** What is in this image? Answer in one concise sentence.
- **Middle sentence:** What is in this image? Answer in 2 sentences.
- **Long sentence:** What is in this image? Answer in three sentences.
- **All sentences:** All length of sentences above.
- **All:** Combines all granularity levels from single nouns to long sentences.

Results indicate that at low granularity, the “**All nouns**” setting achieves the best RE (5.83) and TE (5.45), suggesting that including all nouns provides sufficient information for accurate rotation and translation in simple contexts. At high granularity, “**All sentences**” outperforms others with the lowest TE (3.62) and highest RDA (27.27), indicating that detailed sentences enhance the model’s ability to capture complex relationships. For max granularity, “**Middle sentence**” achieves the highest RDA (81.44), slightly better than “**1 noun**” (81.32), implying that moderate-length sentences effectively balance detail and generality. In terms of mean performance, the “**All**” granularity offers balanced performance, with the best mean RE (4.94), indicating that combining various granularities helps the model generalize better. Additionally, increasing sentence length from “**Short sentence**” to “**Long sentence**” improves RDA under high granularity, demonstrating that longer descriptions capture more details but may introduce slight increases in TE and RE. Overall, finer text granularity using sentences performs better than using only nouns. The performance improvements with sentences significantly enhance the results under high granularity, which consequently improves the overall performance.

**Ablation on swap ratio  $\beta$ .** We conducted additional experiments on the swap ratio  $\beta$  to explore how this parameter affects overall performance, as shown in Tab. B. The results indicate that increasing the swap probability from 0 to 0.7 consistently improves performance. Specifically, the RE decreases from 9.25 to 5.26, the TE decreases from 6.21 to 4.33, and the RDA increases from 16.91 to 23.64. However, when the swap probability exceeds 0.7, performance begins to degrade slightly; RE and TE increase, and RDA decreases.

This suggests that a moderate swap ratio of around 0.7 optimizes the balance between introducing beneficial diversity and avoiding excessive noise in the training data.

### 3.1. More Visual Results

**Qualitative results of granularity.** We conducted experiments to evaluate the impact of text granularity across various datasets, and the results, illustrated in the Figs. D and E, Fig. 4 Fig. C and Fig. B, are consistent performs well. A pattern emerges across all datasets: as the text input becomes more detailed, the pose distribution transitions from a high-variance spread to a narrower, more precise distribution. In parallel, the estimated camera poses increasingly align with the given text input. Notably, when the most fine-grained input, such as an image, is used, our method achieves pose estimations that are the closest to the actual input pose.

**Qualitative results of user study.** We present additional qualitative results demonstrating that the rendered images based on our estimated poses closely match the input text, as shown in Fig. F. In (a), we observe interesting patterns based on the level of detail in the description. For instance, when the prompt "blue car" is given, our method estimates a camera pose at a distinctly different location. In contrast, when the description is more specific and detailed, such as "two bicycles", "tree", "meters", and "map," the estimated pose closely matches the input camera pose. This trend is also evident in (d), where we see a similar pattern: while an overpass is a common feature in urban environments, a dome building is much more unique, leading to more accurate and precise pose estimation.

In (b) and (c), although the estimated camera poses differ significantly from the given input, they still align accurately with the text prompt. For example, in (b), the text condition a "car garage," and the estimated pose even points to a complete parking lot. This highlights the model's ability to generate contextually relevant poses, even when the estimated pose location differs from the input image. In (e), we also report a failure case, which may be attributed to the limitations of the CLIP embedding space when handling long text descriptions, as noted in [69], combined with the inherent complexity of the dataset. In this instance, the estimated pose only partially matches the provided text description. However, in more general scenarios, such as when the text prompt is "bank," the estimated camera successfully identifies another branch of the bank, demonstrating its ability to generalize effectively in less complex cases.

## 4. Discussion and Limitations

To the best of our knowledge, our work is the first to use a diffusion model based on text to estimate pose distributions. Compared to the baseline, our method effectively identifies scenes that match the text description. Additionally, the Gaussian refinement helps us filter out poor samples and

further optimize the pose estimation. Our approach also supports multimodal image inputs. In our experiments, we utilized the Llava model for image captioning at varying granularities. While the model performed well in many cases, we identified a significant limitation when applied to larger and more complex scenes. Specifically, Llava's generated captions were unable to extract and convey sufficiently detailed information necessary for effective scene understanding, particularly in urban environments with dense structures as shown in Fig. A. Given these observations, we recognize the need for more powerful Visual Language Models (VLMs) that can generate richer and more accurate captions, especially for complex and large-scale scenes. As part of our future work, we plan to explore and incorporate more advanced VLMs to improve the quality and granularity of the text descriptions generated, which will ultimately enhance performance in tasks such as scene understanding, localization, and cross-modal retrieval.

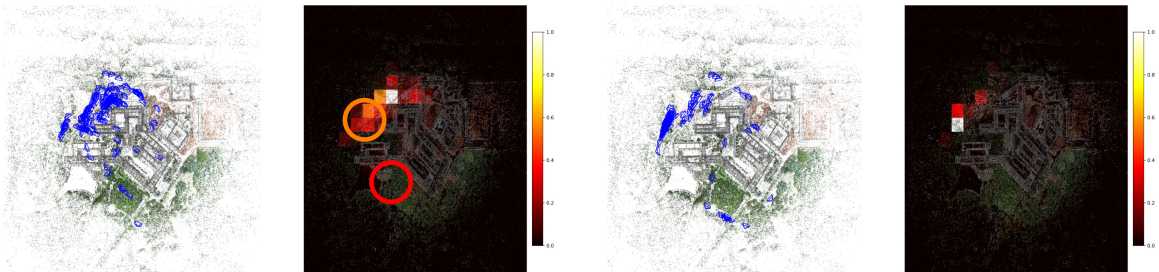
## 5. Broader Impact

The proposed framework for text-based 6DoF camera localization introduces significant advancements in multi-modal reasoning, with potential impacts across various domains. By enabling precise localization based on ambiguous text descriptions, this method could transform applications such as autonomous navigation, urban planning, and augmented reality. For instance, in smart cities, this framework could aid in mapping and localizing critical infrastructure or guiding autonomous vehicles using natural language instructions. Moreover, the integration of text and visual understanding enhances human-robot interaction, making it easier for non-experts to communicate with AI systems in large-scale, complex environments. The ability to perform visual reasoning with 3D Gaussian splatting also sets the stage for more efficient and scalable representations of urban and virtual scenes, benefiting areas like gaming, simulation, and virtual tourism. However, the broad applicability of this technology may also raise ethical concerns, including potential misuse of surveillance or privacy violations. Ensuring the responsible deployment of such systems is essential to mitigate these risks. Overall, this work represents a step forward in bridging natural language understanding with spatial reasoning, paving the way for innovative multi-modal AI applications.



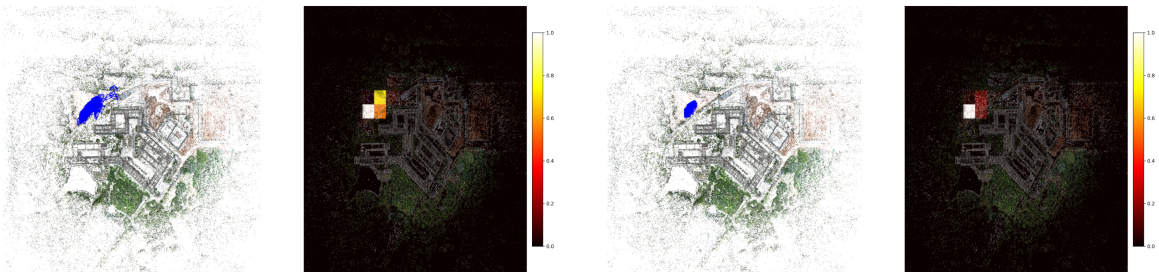
**GT Pose and Image**

**Estimated Pose and Render Image**



**This image shows apartment building.**

**This image shows a large building with many windows and a parking lot in front of it..**

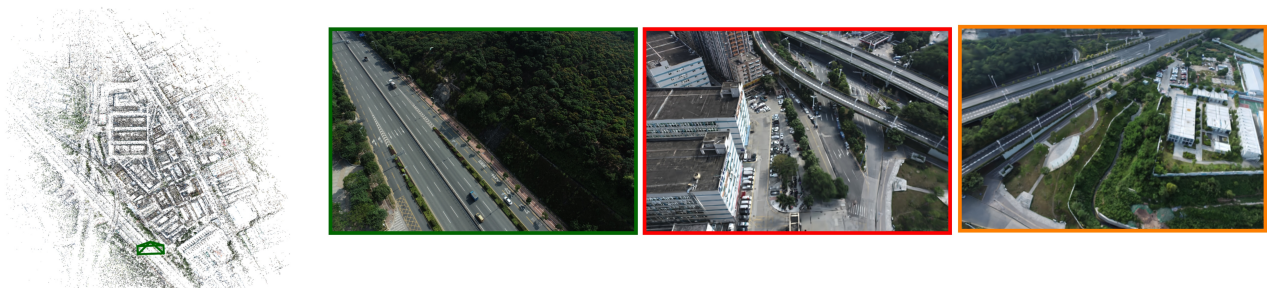


**The image shows a multi-story residential building with a parking lot in front. There are several cars parked in the lot. The building has a mix of red and white exterior walls.**

**< Image CLIP Feature; >**

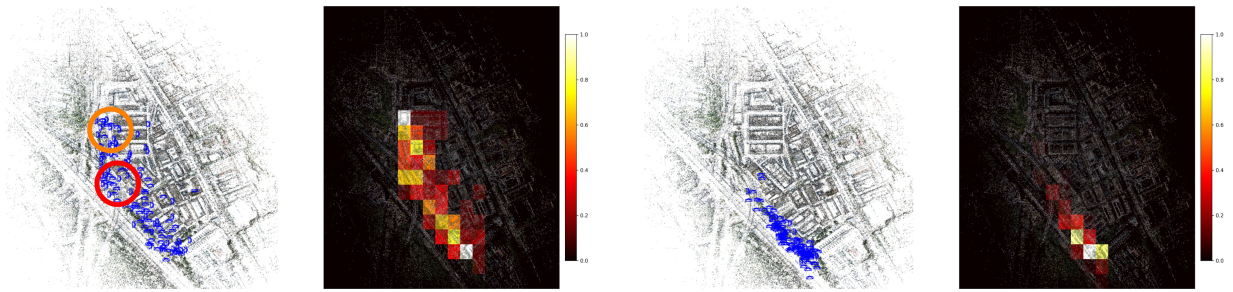
Figure B. **Qualitative Results on the SciArt Dataset:** Similarly, we use the **green camera** to indicate the camera pose used to generate the prompt, while high-density estimations are shown in **orange camera** and **red camera**. Providing more detailed text conditions results in a narrower distribution of estimated camera poses.





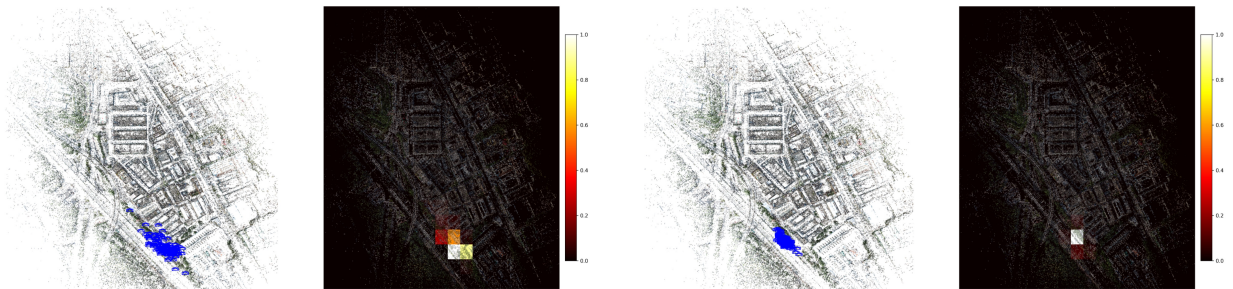
**GT Pose and Image**

**Estimated Pose and Render Image**



**This image shows highway.**

**A highway with cars driving on it, with trees on both sides.**



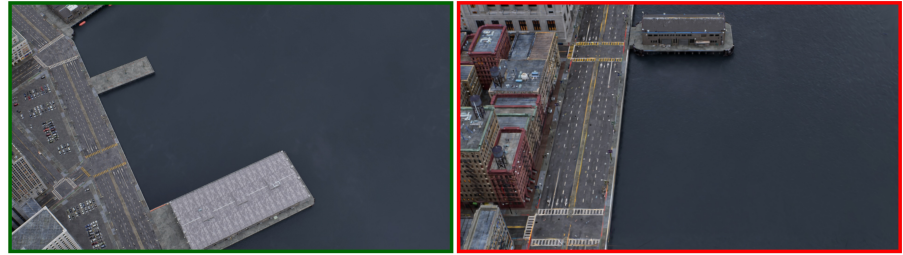
**The image shows a highway with multiple lanes, trees on both sides, and a few vehicles. The highway is elevated above the surrounding landscape, and the shadow indicate a clear sky**

**< Image CLIP Feature; >**

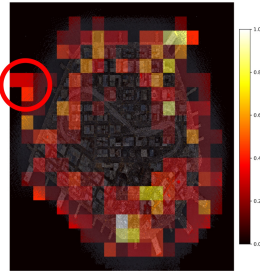
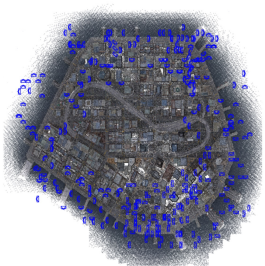
**Figure C. Qualitative Results on the Residence Dataset:** The results demonstrate excellent localization potential. The dataset primarily features a residential area with a highway passing through the left section. When using a general prompt like "The image shows a highway," the estimated camera positions are distributed along the entire highway, successfully aligning with the text prompt. As more detailed information is provided, the estimated positions gradually narrow down and converge closer to the specific locations depicted in the images.



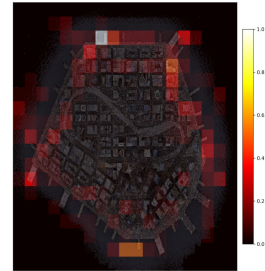
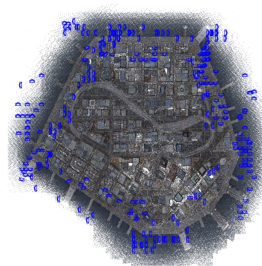
GT Pose and Image



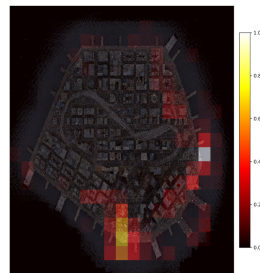
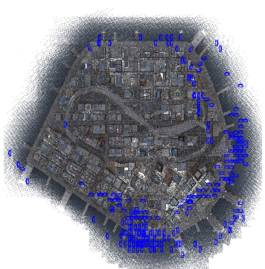
Estimated Pose and Render Image



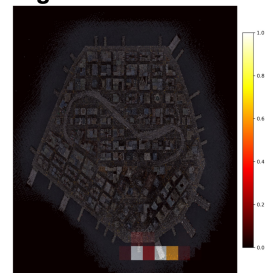
This image shows dock.



The image shows a body of water with a pier extending into it.



The image shows an aerial view of a body of water with a pier extending into it. There is a parking lot on the left side of the image. The water appears calm.



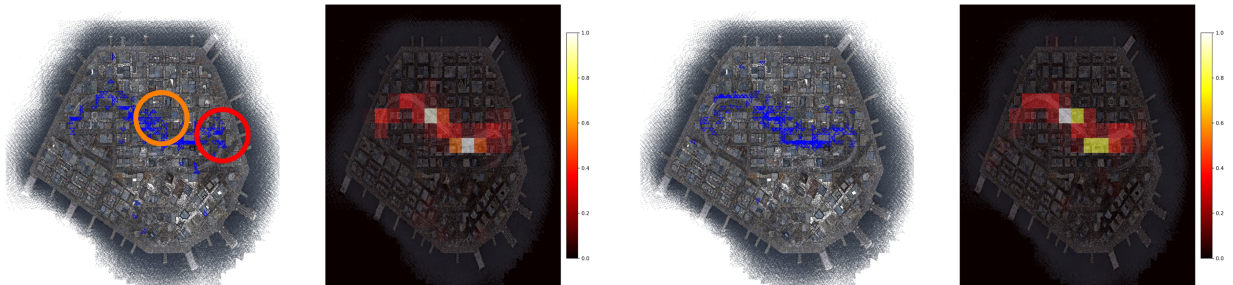
< Image CLIP Feature; >

Figure D. **Qualitative Results on the Matrix City Aerial Dataset:** We observe that our method also performs exceptionally well on large-scale scene datasets. For instance, the **green camera** highlights areas such as a dock and a parking lot. When using simpler or moderately detailed descriptions, the heatmap shows that the estimated poses are distributed across many similar scenes within the city that match the description. However, when the text input includes more specific details, such as mentioning the parking lot, the pose distribution suddenly narrows. The **red renderings** show areas without parking lots, where no poses are present in the estimated distribution.. Finally, when using the given image's CLIP features, we achieve the most accurate pose estimation.



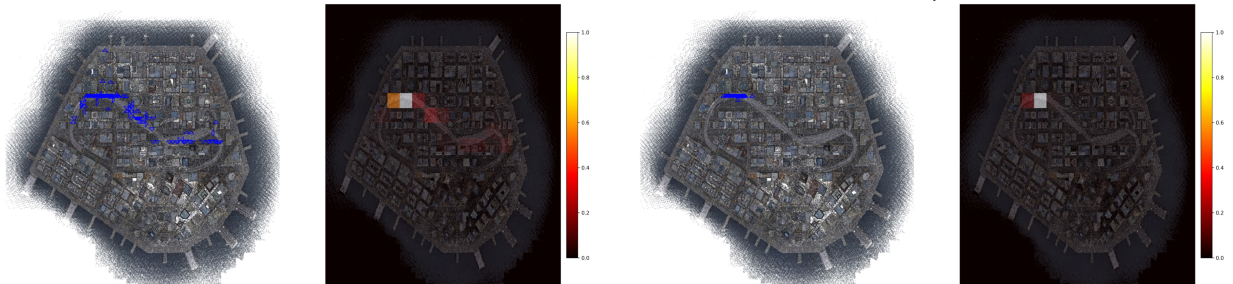
GT Pose and Image

Estimated Pose and Render Image



This image shows parking garage.

This image shows parking garage, concrete, and shadows



The image shows an empty parking garage with graffiti on the walls. The garage is under a concrete structure with a light fixture. The area is fenced off and there are no visible vehicles.

< Image CLIP Feature; >

Figure E. **Qualitative Results on the Matrix City Street Dataset:** On the urban street dataset, most street data is highly similar, with numerous overlapping text inputs. To address this, we used a more distinctive scenario—a garage under an overpass—as the image input. The results show that when we provide a coarse-grained input like "garage," our method generates poses near all potential parking locations, including not only under the overpass but also next to open-air street garages, as indicated by the **red renderings**. We also observe that as the input text becomes more specific, incorporating details like "shadow," "concrete," and "fence off," the distribution variance decreases, and the estimated poses converge closer to the input pose.



a) A blue car parked on the side of a street.



The image shows a bicycle parking area with two bicycles parked at the meters. There is a map and a tree in the background



b) This image shows parking garage.



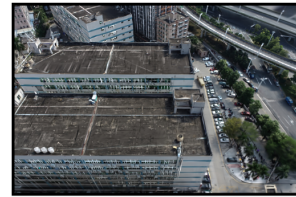
The image shows a construction site with a large building under construction. There is a dirt road leading to the site, and construction materials are visible. The surrounding area includes trees and a building that appears to be undergoing renovation.



c) This image shows rooftop.



The image shows an aerial view of a parking lot with several cars parked. There are also some buildings and a road with vehicles on it. The photo is taken from a high angle, providing a bird's eye perspective of the scene.



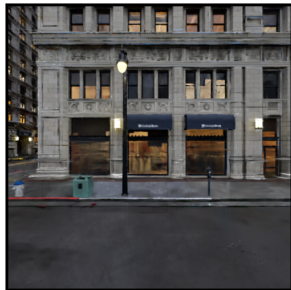
d) This image shows overpass



The image shows a bird's eye view of a cityscape with a prominent dome building in the foreground. The city has a grid-like street pattern and is composed of various buildings of different heights and designs. The architecture suggests a modern urban environment.



e) This image shows bank.



The image shows a bus stop with a shelter and a street sign. There is a large building with reflective glass windows in the background. The street has a number painted on it, indicating a specific location

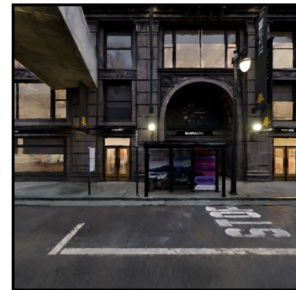


Figure F. Qualitative results of the proposed method: Training images are shown on the left, with the rendered images on the right.